Open Archive TOULOUSE Archive Ouverte (OATAO)

OATAO is an open access repository that collects the work of Toulouse researchers and makes it freely available over the web where possible.

Any correspondence concerning this service should be sent to the repository administrator: staff-oatao@listes-diff.inp-toulouse.fr

A 2-D nucleation-growth model of spheroidal graphite

Jacques Lacaze [a, *], Jacques Bourdie [a, b], Manuel Jesus Castro-Román [c]

[a] CIRIMAT, Université de Toulouse, ENSIACET, CS 44352, 31030 Toulouse Cedex 4, France
[b] Saint-Gobain Pont-à-Mousson, Les Longues Raies, BP 109, 54704 Pont-à-Mousson Cedex, France
[c] CINVESTAV Saltillo, Av. Industria Metalúrgica 1062, Parque Industrial Saltillo-Ramos Arizpe, Ramos Arizpe, Coahuila, 25900, Mexico

A B S T R A C T

Analysis of recent experimental investigations, in particular by transmission electron microscopy, suggests spheroidal graphite grows by 2-D nucleation of new graphite layers at the outer surface of the nodules. These layers spread over the surface along the prismatic direction of graphite which is the energetically preferred growth direction of graphite when the apparent growth direction of the nodules is along the basal direction of graphite. 2-D nucleation-growth models first developed for precipitation of pure substances are then adapted to graphite growth from the liquid in spheroidal graphite cast irons. Lateral extension of the new graphite layers is controlled by carbon diffusion in the liquid. This allows describing quantitatively previous experimental results giving strong support to this approach.

1. Introduction

Graphite spheroids in spheroidal graphite cast iron are known to consist of piling up of graphite layers having their *c* axis oriented parallel to the spheroid radius. To accommodate for the change in orientation in the tangential direction, the spheroids appear to be divided in adjacent sectors which are easily observed by optical microscopy as illustrated in Fig. 1. The change in orientation of the *c* axis at the boundary between two sectors may amount from 10 to several tens of degrees, while the orientation changes within sectors are more limited [1,2].

It has long been recognized that graphite layers within spheroids are arranged in growth blocks which are elongated along the prismatic *a* direction of the graphite structure [3]. This would imply that graphite grows along the prismatic (tangential) direction during spheroidal growth even though the overall (apparent) growth direction is the radial one. Two types of models have been suggested in the past to account for this tangential growth: i) those based on screw dislocations [4] or cone-helix growth [5–7]; and ii) those based on the continuous growth of a graphite layer folding around the spheroid [8,9]. In the first type, tangential growth proceeds around screw dislocations or cones emanating from the

spheroid's centre (Fig. 2-a), giving features that would agree with the observation of sectors. However, transmission electron microscopy (TEM) observations have shown that the orientation of the *c* axis along a sector tilts at random and in either ways [10] which implies that continuous growth around a screw dislocation did not occur. The second type of models (Fig. 2-b) would hardly explain the formation of sectors as already stressed by Gruzleski [9]. However, a slight modification where nucleation of new layers proceeds at the step between two neighbouring sectors which was suggested by Double and Hellawell [11] would (Fig. 2-c).

There has been a renewed interest these last years for investigating the growth mechanism of spheroidal graphite [12–14]. Qing et al. [14] report observation of defects and dislocations in graphite, but do not seem to have observed long range ordered arrangements of these defects that would support the screw dislocation or the cone-helix mechanism. Amini and Abbaschian [12] observed both plate-like and spheroidal growth of graphite in Ni-C samples. They proposed a model for plate-like growth including thickening of the plates by 2-D nucleation and lateral extension of new graphite layers. To explain spheroidal growth, Amini and Abbaschian suggested a roughening transition at the graphite liquid interface which would have no reason for giving sectors as observed. Stefanescu et al. [13] proposed graphite spheroids build-up as so-called tad-pole dendrites. These dendrites emanate from the centre of the spheroids and are made of plate-like growth blocks stack upon each other, though not filling the space as does graphite in spheroids. Considering the model shown in Fig. 2-c and recent TEM
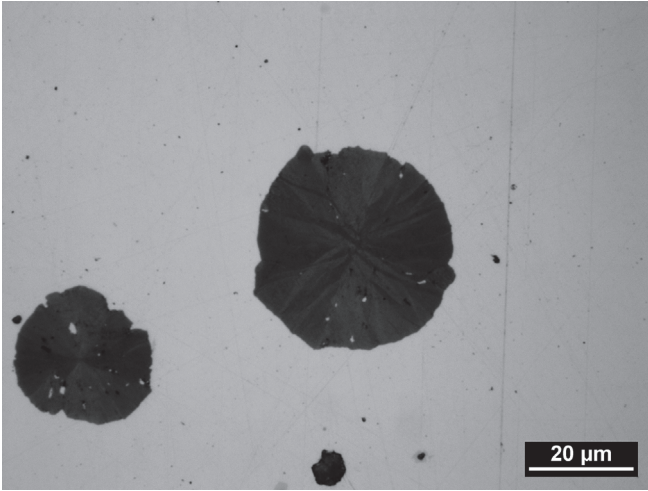

Fig. 1. Optical microscopy micrograph of spheroids showing sectors radiating from the centre.
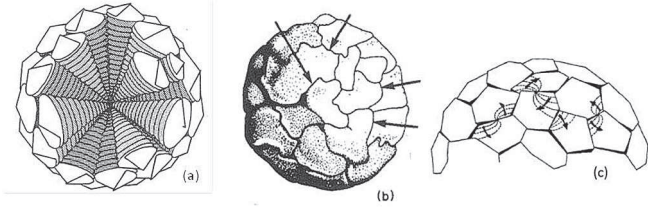

Fig. 2. Schematic of growth of spheroidal graphite following various mechanisms: (a) screw-dislocation [5], (b) cabbage-leaf [9] and (c) 2-D nucleation and lateral extension of graphite layers [11].

observations [2,15] suggest to extend to spheroids the 2-D nucleation and growth model developed by Amini and Abbaschian [12] for plate-like growth of graphite from the liquid. Such an approach has been in fact already suggested based on a simple model [16] and is presented here in a much more formal and quantitative way.

2. 2-D nucleation

Let n be the number of 2-D nuclei per unit area of the graphite/liquid interface. The nucleation rate $J_a = \dot{n} = dn/dt$ is given by Ref. [17]:

$$J_a \approx \frac{N_A}{V_m^l} \cdot \left(\frac{L \cdot \Delta T}{R \cdot T \cdot T_m} \right)^{1/2} \cdot \frac{3 \cdot \beta \cdot D}{2 \cdot a_0} \cdot \exp\left(-\frac{\Delta g^*}{k_B \cdot T} \right) \tag{1}$$

where N_A is Avogadro's number, V_m^l is the molar volume of the liquid, L is the melting enthalpy and T_m the melting temperature, R the gas constant, T the current temperature and $\Delta T = T_m - T$ is the undercooling, β corrects for structural factors [18], D is the diffusion coefficient in the liquid, a_0 is the atomic radius, Δg^* is the excess energy needed for nucleus formation and k_B is Boltzmann's constant. β is expected to take values close to 1 for simple molecules (atoms) and lower than 1 for complex molecules, it will be set to 1 in all the following calculations.

In the above expression, $L \cdot \Delta T / T_m$ is an estimate of ΔG_m, the molar free enthalpy change upon melting of the solid. As suggested by Turnbull and Fisher [19], the fact that graphite precipitates here

from an alloy and not from a pure melt may be accounted for by multiplying J_a by the atomic fraction of carbon, x_C. Equation (1) may thus be written:

$$J_a \approx x_C \cdot \frac{N_A}{V_m^l} \cdot \left(\frac{|\Delta G_m|}{R \cdot T} \right)^{1/2} \cdot \frac{3 \cdot \beta \cdot D}{2 \cdot a_0} \cdot \exp\left(-\frac{\Delta g^*}{k_B \cdot T} \right) \tag{2}$$

Considering nuclei at the surface of a nodule form as discs of radius r and height h, the corresponding free energy change is given as:

$$\Delta g = -\pi \cdot r^2 \cdot h \cdot \frac{|\Delta G_m|}{V_m^{gr}} + 2 \cdot \pi \cdot r \cdot \sigma_e \tag{3}$$

where V_m^{gr} is the graphite molar volume and σ_e is the step energy by length.

Differentiating with respect to r gives the critical value r*:

$$r^* = +\frac{\sigma_e}{h \cdot |\Delta G_m| / V_m^{gr}} \tag{4}$$

and

$$\Delta g^* = +\frac{\pi}{h} \cdot \frac{\sigma_e^2}{|\Delta G_m| / V_m^{gr}} \tag{5}$$

Note that h cannot be determined by this procedure and is most generally considered as being the height of one single atom layer. According to Cahn et al. [18], the step energy per length σ_e is related to the surface energy σ by:

$$\sigma_e = \sigma \cdot a \cdot \sqrt{\xi} \tag{6}$$

where a is the height of one single atom layer and ξ is interface diffuseness which is 1 at most for a sharp interface and can be much smaller in practice [18].

Using the expression for σ_e and setting h = a, one obtains:

$$r^* = +\frac{\sqrt{\xi} \cdot \sigma}{|\Delta G_m| / V_m^{gr}} \tag{7}$$

$$\Delta g^* = +\frac{\pi \cdot a \cdot \xi \cdot \sigma^2}{|\Delta G_m| / V_m^{gr}} \tag{8}$$

Calculations have been made with $x_C = 0.175$ which is the eutectic composition in the Fe-C system, $a = a_0 = 3.51 \cdot 10^{-10}$ m (distance between basal planes), $D = 5 \cdot 10^{-9}$ m$^2 \cdot$s^{-1} as previously selected [20], $\sigma = 1$ J m^{-2} for the prismatic planes (see the review of available data [21]), $V_m^l = 7.5 \cdot 10^{-6}$ m$^3 \cdot$mol^{-1} and $V_m^{gr} = 5.31 \cdot 10^{-6}$ m$^3 \cdot$mol^{-1}, T = 1450 K, and $|\Delta G_m| = 13.64 \cdot \Delta T$ J$\cdot$mol^{-1} [22], where ΔT is the undercooling with respect to the graphite liquidus and is defined positive. One obtains:

$$r^* = \frac{0.4 \cdot \sqrt{\xi}}{\Delta T} \cdot 10^{-6} \text{m} \tag{9}$$

$$\Delta g^* = \frac{4.3 \cdot 10^{-16} \cdot \xi}{\Delta T} \text{J} \tag{10}$$

$$J_a \approx 10^{28} \cdot (\Delta T)^{1/2} \cdot \beta \cdot \exp\left(-\frac{21500 \cdot \xi}{\Delta T} \right) \text{m}^{-2} \cdot \text{s}^{-1} \tag{11}$$

Fig. 3 shows r* and J_a versus ΔT calculated for β set to 1 and ξ set to 0.1, 0.5 and 1. A value of ξ of about 0.1 would seem reasonable as it would give a few hundreds of nuclei per second on the outer

surface of a nodule 10 μm in radius growing at an undercooling of 50 K.

3. Growth kinetics

For describing the effective growth of a faceted crystal along the direction of the facet plane, Cahn et al. [18] and Hillig [17] considered two limits for 2-D nucleation and growth, when either nucleation or spreading of the layers is controlling.

In the first case, it is considered that a new layer nucleates only when the previous layer has spread over the corresponding crystal facet, this is the so-called MNG (mono-layer growth) process [23]. Following Tiller [24], we can ask the question: "What is the radius of disk, R, of a crystal facet which has unit probability that a new nucleus will form on top of the disk in the time τ that it takes to the original disk to grow to its maximal extension?" Assuming a constant ledge velocity, one then has:

$$J_a \cdot \left(\pi \cdot R^2 \right) \cdot \tau = 1 \tag{12}$$

For the present case, we shall consider that the crystal facet is the outer surface of a sector. If a nodule of radius R_G has N_S similar sectors, then:

$$\tau = \frac{N_S}{J_a \cdot \left(4 \cdot \pi \cdot R_G^2 \right)} \tag{13}$$

Within this time interval τ, N_S new nuclei are expected to spread over the surface of the N_S sectors, i.e. on a distance that scales as $L_S = 2 \cdot R_G \cdot \sqrt{\pi / N_S}$. Fig. 4 illustrates the change of τ versus undercooling (with respect to graphite liquidus) for $\xi = 0.1$, $N_S = 100$ and R_G set to 1, 10 and 50 μm. When the nucleation rate becomes reasonable — at an undercooling larger than 50 K as seen above — the corresponding spreading time becomes so small that this model does not seem to be appropriate. This has been emphasized by plotting on the same graph the corresponding spreading
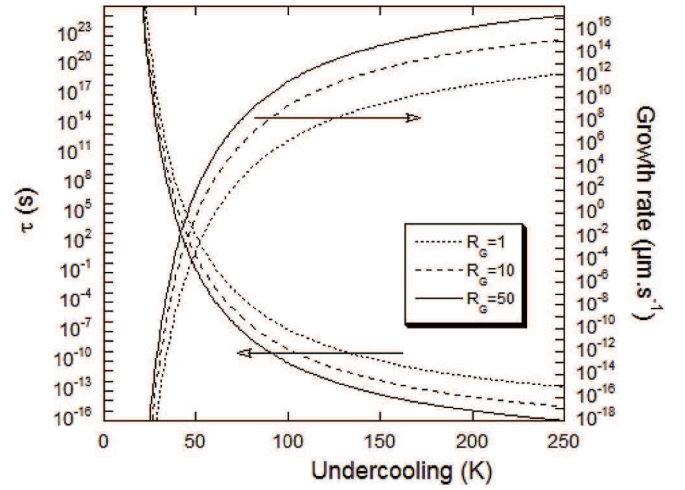

Fig. 4. Evolution with undercooling of the time interval between nucleation events and of the corresponding spreading velocity for three spheroid radii R_G (indicated in microns in the figure) according to the MNG model.

velocity, which becomes unphysically high for undercoolings higher than 50 K. This trend is certainly related to the fact that the far field diffusion of carbon is not accounted for by the model which was derived for precipitation in pure melts.

The other alternative is the so-called PNG (poly-layer growth) mechanism [23] that is controlled by the growth rate and not by the nucleation rate. The growth rate G is now given as [17]:

$$G_{PNG} = a \cdot \left(\frac{\pi}{3} \cdot J_a \cdot (V_l)^2 \right)^{1/3} \tag{14}$$

where V_l is the spreading rate of the ledge and has been here assumed constant. Other exponents and relations could be obtained when using different laws for spreading rate [23].
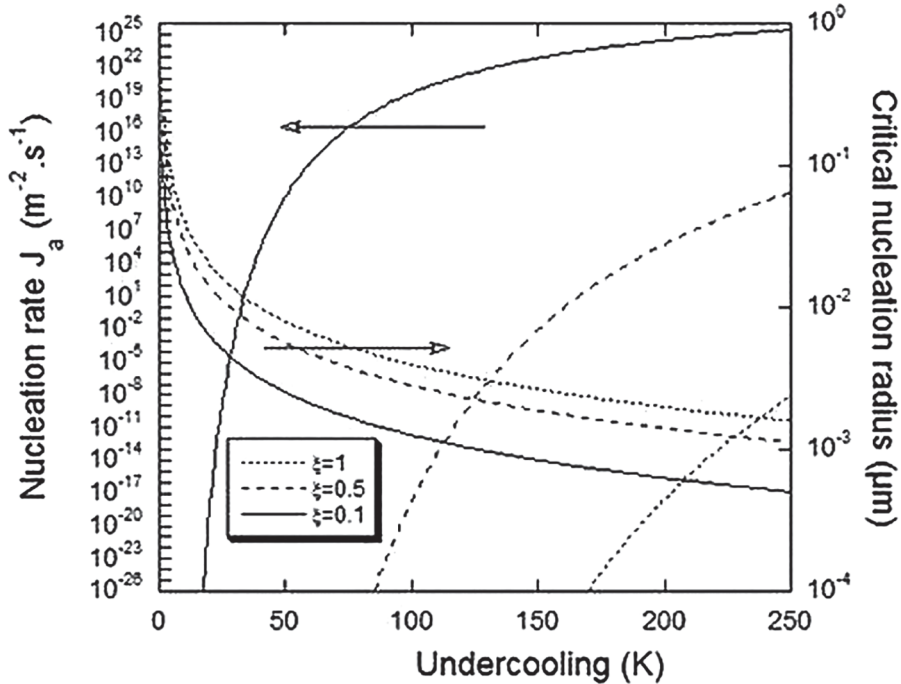

Fig. 3. 2-D nucleation rate and radius of the critical nuclei versus undercooling (with respect to graphite liquidus) for three values of ξ.

If there is no constraint, V_l can be expressed as its value for a straight ledge V_∞, which is according to Cahn et al. [18]:

$$V_\infty = \frac{D \cdot |\Delta G_m|}{h \cdot R \cdot T} \cdot \beta \cdot \left(2 + \xi^{-1/2}\right) \tag{15}$$

Inserting this latter expression in Equation (14), one obtains for the PNG process with h = a:

$$G_{PNG} = \left(\frac{\pi}{2} \cdot x_C \cdot \frac{N_A}{V_m^l}\right)^{1/3} \cdot \left(\frac{|\Delta G_m|}{R \cdot T}\right)^{5/6} \cdot \beta \cdot \left(2 + \xi^{-1/2}\right)^{2/3} \cdot D \cdot \exp\left(-\frac{\Delta g^*}{3 \cdot k_B \cdot T}\right) \tag{16}$$

With the values already used, G_{PNG} becomes:

$$G_{PNG} \approx 0.05 \cdot (\Delta T)^{5/6} \cdot \beta \cdot \left(2 + \xi^{-1/2}\right)^{2/3} \cdot \exp\left(-\frac{7200 \cdot \xi}{\Delta T}\right) m \cdot s^{-1} \tag{17}$$

Fig. 5 shows with dotted lines the evolution of G_{PNG} according to equation (17) for β set to 1 and ξ set to 0.1, 0.5 and 1. The horizontal interrupted line corresponds to the experimental thickening rate of graphite plates along their **c** direction as estimated by Amini and Abbaschian [12]. This value of 0.1 μm s⁻¹ is obtained for an undercooling of 40 K at ξ = 0.1 and 200 K at ξ = 0.5, both values being well within the reported experimental range [12] of undercooling values with respect to graphite liquidus.

For the same reason than for the MNG model, the PNG model is expected to predict too high growth rates. There is an alternative approach to express V_∞ which appears more convenient in the case of alloys. Following Amini and Abbaschian [12], V_∞ in the above treatment could as well be estimated as the diffusion-controlled growth rate of a plate of thickness 2·ρ. The validity of such an approach has been discussed by Doherty [25]. Amini and Abbaschian made use of a Zener-type formulation which gives [26]:
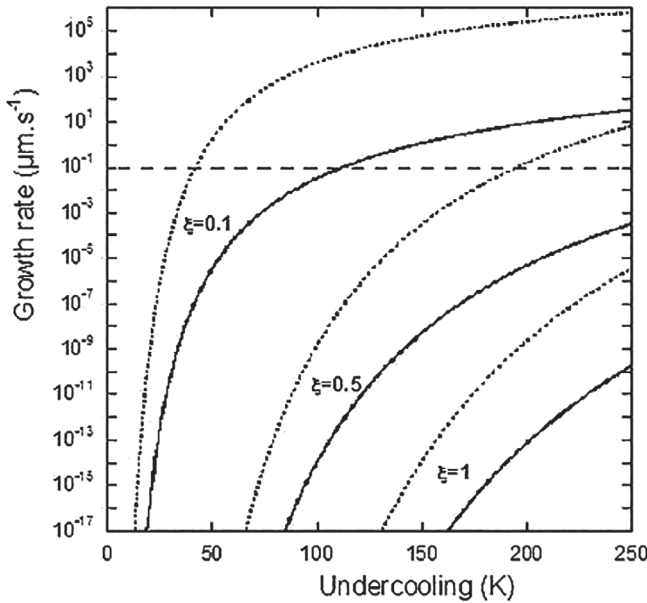

Fig. 5. Overall growth rate of a graphite spheroid according to the PNG model as function of undercooling, for three values of ξ. Dotted lines are according to equation (17) and solid lines to equation (29). The horizontal line corresponds to the experimental thickening rate of graphite plates estimated by Amini and Abbaschian [12].

$$V_\infty = \frac{D}{k} \cdot \frac{V_m^{gra}}{V_m^l} \cdot \left(\frac{x_C^{l,0} - x_C^i}{x_C^{gra} - x_C^i}\right) \cdot \frac{1}{\rho} \cdot \left(1 - \frac{\rho^*}{\rho}\right) \tag{18}$$

where $x_C^{l,0}$, x_C^i and x_C^{gra} are the carbon mole fraction in the bulk liquid, at the liquid graphite interface and in graphite respectively. ρ^* is the critical curvature radius of the plate tip that would cancel the composition difference $(x_C^{l,0} - x_C^i)$. k is a constant of order unity, set to 1 by Amini and Abbaschian but to 2 by Hillert [26].

ρ^* will be here considered as the critical radius for homogeneous nucleation:

$$\rho^* = +\frac{2 \cdot \sigma}{|\Delta G_m|/V_m^{gra}} \tag{19}$$

Using the usual Zener's proposal, the plate grows at the maximum possible rate which corresponds to $\rho = 2 \cdot \rho^*$, so that for k set to 2:

$$V_\infty = \frac{D}{8 \cdot \rho^*} \cdot \frac{V_m^{gra}}{V_m^l} \cdot \left(\frac{x_C^{l,0} - x_C^i}{x_C^{gra} - x_C^i}\right) \tag{20}$$

According to the Fe-C phase diagram, $x_C^{l,0} - x_C^i \approx \Delta T/11900$ where ΔT is the undercooling with respect to graphite liquidus close to the eutectic composition. With $x_C^{gra} = 1$ and x_C^i approximated to the eutectic composition, i.e. $x_C^i = 0.175$, and all other values as before, V_∞ can be expressed as:

$$V_\infty = 6.0 \cdot 10^{-8} \cdot (\Delta T)^2 m \cdot s^{-1} \tag{21}$$

At an undercooling of 50 K, this expression leads to a growth rate of 150 μm s⁻¹ which is two orders of magnitude higher than the steady state value reported by Amini and Abbaschian [12]. In fact, these authors did introduce a value of 5 μm for h* instead of the calculated value of ρ^*, and this explains most of the discrepancy between the two estimates.

Alternatively, the growth rate V_∞ of the plate could be calculated using the model developed by Trivedi [27] which relates the Péclet number $P = \rho \cdot V_\infty/2 \cdot D$, to the dimensionless supersaturation, $\Omega_0 = (x_C^{l,0} - x_C^i)/(x_C^{gra} - x_C^i)$. With the values given above, $\Omega_0 = 10^{-4} \cdot \Delta T$ and is small enough for any reasonable undercooling that the approximate solution worked out by Bosze and Trivedi [28] may be used. According to this solution, one has:

$$\frac{\rho^*}{\rho} = \frac{3}{32} \cdot \Omega_0 \tag{22}$$

and

$$P = \frac{9}{16 \cdot \pi} \cdot (\Omega_0)^2 \tag{23}$$

With further mathematical manipulations, Bosze and Trivedi arrived at:

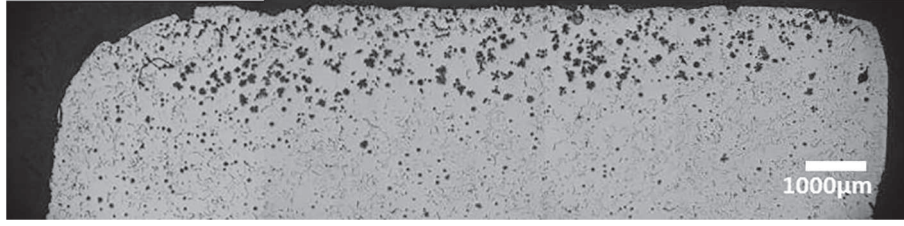$$V_\infty = \frac{9}{8 \cdot \pi} \cdot \frac{D}{\rho} \cdot (\Omega_*)^2 \tag{24}$$

Fig. 6. Upper part of the metallographic section of a sample cooled at 20 °C/min.

where Ω_* is given as:

$$\Omega_* = \frac{\Omega_0}{1 - \frac{2}{\pi}\cdot\Omega_0 - \frac{1}{2\cdot\pi}\cdot(\Omega_0)^2} \tag{25}$$

Bosze and Trivedi stressed the fact that the solution thus obtained is valid over a quite large range of supersaturation values. Here however, we can restrict ourselves to low supersaturation values for which $\Omega_* \approx \Omega_0$. It is then of interest to compare the two above expressions (equations (20) and (24)) of the growth rate by expressing their ratio. Without considering the change in molar volume, this ratio writes:

$$\frac{V_\infty^{Zener}}{V_\infty^{Bosze}} = \frac{8\cdot\pi}{9\cdot k}\cdot\frac{1}{\Omega_0}\cdot\left(1 - \frac{\rho^*}{\rho}\right) \tag{26}$$

This ratio scales as $(\Omega_0)^{-1}$ indicating the Zener-type model can strongly overestimate the growth rate in the present case and thus that equation (24) is certainly to be preferred. Inserting the expression of ρ^* in the above final relation of Bosze and Trivedi gives:

$$V_\infty = \frac{27}{256\cdot\pi}\cdot\frac{D}{\rho^*}\cdot(\Omega_0)^3 \tag{27}$$

With the same numerical values as before this writes:

$$V_\infty \approx 2\cdot10^{-16}\cdot(\Delta T)^4 m\cdot s^{-1} \tag{28}$$

The overall growth rate G of a nodule of radius R_G from the liquid is now calculated according to the PNG model. After insertion of the appropriate values in equation (14), one obtains:

$$G_{PNG} = 2.6\cdot10^{-11}\cdot(\Delta T)^{17/6}\cdot(\beta)^{1/3}\cdot\exp\left(-\frac{7200\cdot\xi}{\Delta T}\right) m\cdot s^{-1} \tag{29}$$

The solid lines in Fig. 5 show the evolution of G_{PNG} according to equation (29) for β set to 1 and ξ set to 0.1, 0.5 and 1 as before. As expected, the predicted values are much lower than those calculated with equation (17) at any undercooling. Interestingly enough, it is seen that the G_{PNG} value for $\xi = 0.1$ levels out in the range of undercoolings of interest.

4. Application

As a check of the appropriateness of the above approach, it was applied to previously reported results [16]. In these experiments, a sample (8 mm in diameter, 10 mm in height) of cast iron with 3.75 wt.% C and 2.7 wt.% Si was remelted in graphite crucibles by heating up to 1350 °C. The cast iron had been spheroidized with a slight over-treatment in magnesium for allowing short remelting. However, to avoid too large magnesium loss which would have hindered spheroidal growth during solidification, the samples were cooled immediately after reaching 1350 °C. Two cooling rates were used, 20 °C/min (referred as "slow" cooling rate afterwards) or 350 °C/min (referred as "high" cooling rate). Before introducing a sample in the crucible, some commercial inoculant amounting to 0.2% of the weight of the sample was located at the bottom of the crucible.

After processing, the samples were sectioned along a vertical axial section and prepared for metallographic observations. Fig. 6 shows an example of the upper surface of one sample cooled at 20 °C/min. Large spheroids are seen to have grown and floated while the remaining of the sample consisted in a standard microstructure of a spheroidized cast iron. The large spheroids are expected to have nucleated at the bottom of the sample as soon as the metal started to cool from 1350 °C and to have grown freely in the liquid until the bulk of the material solidified as the eutectic temperature was reached. If an eutectic undercooling of 10−20 °C is considered, this latter temperature must have been about 1150 °C. Accordingly, the time for growth of the graphite precipitates from the liquid was about 34 s and 600 s for fast and slow cooling respectively.

The half-size of the five largest precipitates of the two samples was then measured for comparison with predicted spheroid radius. These measurements are reported in Fig. 7 as rectangles showing the scatter of the data.

At the start of cooling, the liquid is assumed saturated in carbon at a level corresponding to 1350 °C. Then, during primary graphite growth, its carbon content x_C^l decreases. This must be accounted for in the calculations by tracking the evolution of the undercooling with respect to graphite liquidus. At any time during cooling, the change dx_C^l of x_C^l is obtained from a carbon balance as:
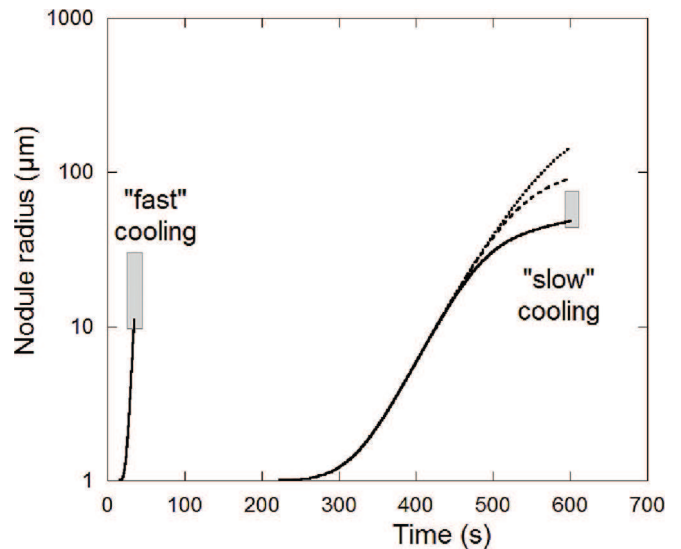

Fig. 7. Time evolution of primary graphite spheroids in a melt cooled at a rate of 20 °C/min (slow cooling) or 350 °C/min (fast cooling).

$$dx_C^l = -\frac{\frac{V_m^l}{V_m^{gra}} \cdot x_C^{gra} - x_C^l}{1 - g^{gra}} \cdot dg^{gra} \qquad (30)$$

where g^{gra} and dg^{gra} are the volume fraction of graphite and its derivative. One has:

$$dg^{gra} = 4 \cdot \pi \cdot N^{gra} \cdot (R_G)^2 \cdot dR_G \qquad (31)$$

in which N^{gra} is the number density of graphite spheroids.

At each time step, the value of ΔT is thus updated according to the new value of x_C^l. Owing to the very limited number of primary spheroids that were observed at the top of the samples (Fig. 6), low values of N^{gra} were considered, namely 0.01, 0.1 and 1 mm^{-3}. The calculated evolution with time of the spheroids radius is plotted in Fig. 7. In the case of fast cooling, changing the nodule count within the range considered had no effect and all three curves are superimposed. On the contrary, in the case of slow cooling, increasing the nodule count increases carbon pick up from the liquid and thus leads to a decrease of the final spheroids size. Comparison of the present calculations with experimental measurements shows a fair agreement when N^{gra} is between 0.1 and 1 mm^{-3}.

5. Conclusion

Reviewing past and recent experimental information on spheroidal graphite growth in cast iron suggests it grows by continuous 2-D nucleation and lateral extension of graphite layers at the outer surface of the nodules. A model corresponding to such a schematic has been derived for graphite precipitation from the liquid using a classical 2-D nucleation law and various laws for lateral extension of the new steps. Amongst these latter, the description based on growth controlled by carbon diffusion in the liquid gives satisfactory predictions when compared to experimental observations. In these models, values for all physical parameters are from literature information but interface diffuseness. Future extension of this approach is sought for accounting for the effect of impurities on lateral extension of the growth steps following previous approaches [29,30].

References

[1] K. Theuwissen, J. Lacaze, M. Véron, L. Laffont, Nano-scale orientation mapping of graphite in cast irons, Mater. Charact. 95 (2014) 187−191.
[2] K. Theuwissen, J. Lacaze, L. Laffont, Structure of graphite precipitates in cast iron, Carbon 96 (2016) 1120−1128.
[3] R. Mitsche, G. Haensel, K. Maurer, H. Schäffer, Recherches, par examen au microscope électronique notamment, sur les formes dégénérées du graphite dans les fontes G.S, Fonderie 270 (1968) 367−382.
[4] M. Hillert, Y. Lindblom, The growth of nodular graphite, J. Iron Steel Inst. 148 (1954) 388−390.
[5] D.D. Double, A. Hellawell, Cone-helix growth forms of graphite, Acta Metal. 22 (1974) 481−487.
[6] Baihe Miao, Keming Fang, Weimin Bian, Guoxun Liu, On the microstructure of graphite spherulites in cast irons by TEM and HREM, Acta Metal. Mater. 38 (1990) 2167−2174.
[7] Baihe Miao, D.O. Northwood, Weimin Bian, Keming Fang, Minz Heng Fan, Structure and growth of platelets in graphite spherulites in cast iron, J. Mater. Sci. 29 (1994) 225−261.
[8] J.P. Sadocha, J.E. Gruzleski, The mechanism of graphite spheroid formation in pure Fe-C-Si alloys, in: B. Lux, I. Minkoff, F. Mollard (Eds.), The Metallurgy of Cast Iron, Georgi Publishing Company, St. Saphorin, 1975, pp. 443−456.
[9] J.E. Gruzleski, On the growth of spherulitic graphite in nodular cast iron, Carbon 13 (1975) 167−173.
[10] J. Lacaze, K. Theuwissen, L. Laffont, M. Véron, Misorientations in spheroidal graphite: some new insights about spheroidal graphite growth in cast irons, IOP Conf. Ser. Mater. Sci. Eng. 117 (2016) 012024, http://dx.doi.org/10.1088/1757-899X/117/1/012024.
[11] D.D. Double, A. Hellawell, The nucleation and growth of graphite. The modification of cast iron, Acta Metal. Mater. 43 (1995) 2435−2442.
[12] S. Amini, R. Abbaschian, Nucleation and growth kinetics of graphene layers from a molten phase, Carbon 51 (2013) 110−123, http://dx.doi.org/10.1016/j.carbon.2012.08.019.
[13] D.M. Stefanescu, G. Alonso, P. Larranaga, E. De la Fuente, R. Suarez, On the crystallization of graphite from liquid iron-carbon-silicon melts, Acta Mater. 107 (2016) 102−126, http://dx.doi.org/10.1016/j.actamat.2016.01.047.
[14] J. Qing, V.L. Richards, D.C. Van Aken, Growth stages and hexagonal-rhombohedral structural arrangements in spheroidal graphite observed in ductile iron, Carbon 116 (2017) 456−469, http://dx.doi.org/10.1016/j.carbon.2017.01.063.
[15] Dongdong Li, Ruixuan Tan, Jingxing Gao, Bingqiang Wei, Zheqiong Fan, Qizhong Huang, Kejian He, Comparison of pyrolitic graphite spheres from propylene with spheroidal graphite nodules in steel, Carbon 111 (2017) 428−438, http://dx.doi.org/10.1016/j.carbon.2016.10.018.
[16] R. Ghergu, L. Magnusson Åberg, J. Lacaze, A possible mechanism for the formation of exploded graphite in nodular cast irons, Mater. Sci. Forum 790−791 (2014) 435−440, http://dx.doi.org/10.4028/www.scientific.net/MSF.790-791.435.
[17] W.B. Hillig, A derivation of classical two-dimensional nucleation kinetics and the associated crystal growth laws, Acta Metall. 14 (1966) 1868−1869.
[18] J.W. Cahn, W.B. Hillig, G.W. Sears, The molecular mechanism of solidification, Acta Metall. 12 (1964) 1421−1439.
[19] D. Turnbull, J.C. Fisher, Rate of nucleation in condensed systems, J. Chem. Phys. 17 (1949) 71−73.
[20] J. Lacaze, G. Lesoult, M. Castro, Solidification of spheroidal graphite cast iron. Part II : numerical simulation, Acta Mater. 46 (1998) 997−1010.
[21] U. de la Torre, J. Lacaze, J. Sertucha, Chunky graphite formation in ductile cast irons: effect of silicon, carbon and rare earths, Int. J. Mater. Res. 107 (2016) 1041−1050, http://dx.doi.org/10.3139/146.111434.
[22] M. Hillert, V.V. Subba Rao, Grey and White Solidification of Cast Iron, The Institute of Metals, ISI P110, pp. 204−212.
[23] S.D. Peteves, R. Abbaschian, Growth kinetics of solid-liquid Ga interfaces: Part II. Theoretical, Metall. Trans. A 22A (1991) 1271−1286.
[24] W.A. Tiller, The Science of Crystallization − Microscopic Interfacial Phenomena, Cambridge University Press, 1991, pp. 81.
[25] R.D. Doherty, B. Cantor, Computer modelling of ledge growth kinetics, in: H.I. Aaronson (Ed.), Solid-state Phase Transformations, Met. Soc. AIME, Warrendale, 1982, pp. 547−553; and R.D. Doherty, Diffusive phase transformations in the solid state, in: R.W. Cahn, P. Haasen (Eds.), Physical Metallurgy, Elsevier Science Publishers, 1983, pp. 933−1030.
[26] M. Hillert, The role of interfacial energy during solid state phase transformations, Jernkont. Ann. 141 (1957) 757−789.
[27] R. Trivedi, The role of interfacial free energy and interface kinetics during the growth of precipitate plates and needles, Metall. Trans. 1 (1970) 921−927.
[28] W.P. Bosze, R. Trivedi, On the kinetic expression for the growth of precipitate plates, Metall. Trans. 5 (1974) 511−512.
[29] N. Cabrera, D.A. Vermilyea, The growth of crystals from solution, in: R.H. Dorelus (Ed.), Growth and Perfection of Crystals, Int. Conf. On Crystal Growth, Wiley and Sons, 1958, pp. 393−410.
[30] N. Albon, J. Dunning, Growth of sucrose crystals: determination of edge energy from the effect of added impurity on rate of step advance, Acta Cryst. 15 (1962) 474−476.